Single-Satellite Lunar Navigation via Doppler Shift Observables for the NASA Endurance Mission

Kaila M. Y. Coimbra, Marta Cortinovis, Tara Mina, and Grace Gao, *Stanford University*

BIOGRAPHY

Kaila M. Y. Coimbra is a Ph.D. student in the Department of Aeronautics and Astronautics at Stanford University. She received her B.S. in Mechanical Engineering, with a minor in Aerospace Engineering, from the California Institute of Technology. Her research interests include positioning, navigation, and timing, particularly for lunar surface rovers.

Marta Cortinovis is a Ph.D. candidate in the Department of Aeronautics and Astronautics at Stanford University. They received their B.S. in Aerospace Engineering in 2022 from the University of Illinois Urbana-Champaign. Their research interests include position, navigation, and timing, space systems, and robotics.

Tara Mina is a research engineer at Georgia Tech in the Space Exploration Analysis Laboratory. She received her Ph.D. in the Electrical Engineering Department from Stanford University in 2023. Prior to that, she obtained her B.S. in Electrical Engineering from Iowa State University in 2017 and her M.S. in Electrical and Computer Engineering from the University of Illinois at Urbana-Champaign in 2019. Her research interests include secure positioning, navigation, and timing (PNT), GNSS signal design, lunar PNT, and optical navigation for space exploration.

Grace Gao is an Associate Professor in the Department of Aeronautics and Astronautics at Stanford University. She leads the Navigation and Autonomous Vehicles Laboratory (NAV Lab). Before joining Stanford University, she was faculty at University of Illinois at Urbana-Champaign. She obtained her Ph.D. degree at Stanford University. Her research is on robust and secure perception, localization and navigation with applications to manned and unmanned aerial vehicles, autonomous driving cars, as well as space robotics.

ABSTRACT

Set to launch in the 2030s, the NASA Endurance rover will explore and collect samples along a $2000\ \mathrm{km}$ traverse of the Moon's South Pole-Aitken (SPA) impact basin. Precise geotagging of these samples will be critical to the mission's science objectives, which aim to characterize the Solar System's chronology and the Moon's geological evolution. Concurrently, the Surrey Satellite Technology Ltd. (SSTL) will be launching the Lunar Pathfinder satellite to provide communication services to lunar surface users, including the Endurance rover. To enable precise absolute localization of the rover throughout its $2000\ \mathrm{km}$ traverse, we investigate the achievable position estimation by opportunistically leveraging the Doppler shift observables from the Lunar Pathfinder's downlink communication signals with no navigation payload.

With only one satellite available, we accumulate Doppler shift measurements over time while the rover is stationary and refine the rover's position estimate through a weighted batch filter framework. In simulation, we model the effects of Doppler shift measurement uncertainty, which includes the frequency error of the rover's clock as well as errors due to carrier tracking as a function of the carrier-to-noise ratio C/N_0. The state estimation performance is evaluated at different key locations of the SPA basin under varying degrees of satellite ephemeris uncertainty and clock stability. With this framework of using Doppler shift as the only navigation observable, we find that the Lunar Pathfinder is, on average, able to opportunistically localize the Endurance rover with sub-$10\text{-}\mathrm{m}$ accuracy within two orbital periods of the Lunar Pathfinder. To the best of the author's knowledge, this paper is the first to examine lunar localization using a single satellite that is not equipped with a navigation payload.

I. INTRODUCTION

NASA is actively working toward establishing a permanent human presence on the Moon and in cislunar space through the Artemis program (NASA, 2022). To facilitate eventual human exploration and long-term stay, the NASA Jet Propulsion Laboratory (JPL) has been developing autonomous exploratory rover missions to study the lunar South Pole. One of these mission concepts is Endurance, a long-range lunar rover that aims to collect and return surface samples from the South-Pole Aitken (SPA) impact basin (Keane et al., 2022). These samples will provide key insights into the Solar System's chronology and characterize the geologic diversity of the largest and oldest impact basin on the Moon. The Endurance rover will be collecting these samples from key waypoints that are distributed across its planned $2000\ \mathrm{km}$ long traverse.

1. Related Works

In order to properly geotag the samples, precise absolute localization of the rover is critical. For most planetary rover missions including Endurance, the global localization error requirement is $10\ \mathrm{m}$ (Cauligi et al., 2023). Currently, JPL has proposed two vision-based techniques for localization: LunarNav and ShadowNav. LunarNav involves autonomous crater detection using onboard cameras and matching of the craters to a developed database of lunar features that are mapped from satellite imagery (Daftry et al., 2023). Under the scenario where Endurance is not in a sunlit area, ShadowNav detects shadows from crater edges and matches the shadows to the onboard map (Cauligi et al., 2023). While the positioning errors for both techniques are within the localization error requirement of $10\ \mathrm{m}$, both methods are computationally expensive and memory intensive since they require Endurance to autonomously run visual matching algorithms as well as store the maps onboard. Furthermore, its positioning accuracy is highly dependent on the quality of the maps' resolution.

Multiple satellite-based localization strategies have also been investigated for lunar surface applications. Prior works have shown that weak terrestrial GPS signals reaching cislunar space can be utilized for absolute positioning on the lunar surface (Iiyama et al., 2023). However, given that the SPA impact basin is on the far side of the Moon, GPS sidelobe signals will not be accessible to the Endurance rover during its mission (Keane et al., 2022). Jun et al. (2023) have proposed a Joint Doppler and Ranging approach, which has achieved sub-10-m level positioning accuracy with two lunar satellites. This approach requires a lunar reference station within $15\ \mathrm{km}$ of the user, which is not feasible for the $2000\ \mathrm{km}$ traverse planned for Endurance. Cortinovis et al. (2024) assess the achievable localization accuracy of the Endurance rover using a single satellite, the Lunar Pathfinder satellite, assuming it is equipped with a radiometric navigation payload. The two-way ranging method proposed in Cortinovis et al. (2024) was successful in achieving sub-10-m level positioning accuracy within $4\ \mathrm{hours}$. However, in the time frame of the Endurance mission, it is likely that the Lunar Pathfinder will not have a navigation payload to provide ranging observables and will only provide communication services for lunar surface users (SSTL, 2022). Therefore, these constraints on the mission scenario motivate this work to investigate using the already-available downlink communication signals to opportunistically extract navigation observables. In this paper, we investigate a framework to provide absolute localization for the Endurance rover using Doppler shift observables from a single satellite that is not equipped with a navigation payload.

Prior navigation systems that employed Doppler shift measurements include TRANSIT, the first satellite navigation system ever implemented. TRANSIT was conceptualized in the late 1950s and became operational in the mid-1960s. Due to the low number of satellites that were deployed for TRANSIT, the system was primarily intended to update the position of resurfaced submarines that were stationary for hours or days at a time. TRANSIT was able to localize within $5\ \mathrm{m}$ for 3D positioning accuracy if the receiver was stationary for several days (Misra and Enge, 2012). More recently, exploiting signals of opportunity from large Low Earth Orbit (LEO) constellations have been of interest to the navigation community. In Psiaki (2021), aptly named "TRANSIT on steroids," the author identifies that large LEO constellations, such as OneWeb, Starlink, and Kuiper, will not have the capabilities to send pseudorange measurements. By utilizing the carrier Doppler shift of these downlink signals, Psiaki (2021) demonstrates sub-5-m level positioning accuracy can be achieved with the LEO satellite constellations. This multi-satellite scenario enables the accumulation of multiple measurements simultaneously. In contrast, the single-satellite scenario presented in this paper necessitates the accumulation of measurements over time to ensure sufficient geometric diversity in the measurements, much like the original TRANSIT system's mode of operation. The TRANSIT navigation system assumes that the clock onboard the satellite and user is stable enough that the clock drift is constant over the measurement window (Kershner and Newton, 1962). In this paper, we also assume that the rover's clock drift is constant over the measurement window, and that the satellite's clock is stable.

2. Proposed Approach

In this work, we leverage the communication signal from the Lunar Pathfinder to localize the Endurance rover. We assume that the rover remains stationary while obtaining a positioning fix and that it is equipped with a clock that has a constant drift over the measurement window. A flow chart of the high-level approach proposed in this paper is shown in Figure 1.

Given the specifications of the satellite's communication signal (SSTL, 2022), we simulate Doppler shift measurements received by the Endurance rover at key waypoints along the rover's path. For localization, we accumulate these Doppler measurements over time, which the receiver is able to obtain using a phase locked loop (PLL). The Doppler shift measurement model takes into account uncertainty from ephemeris errors, the rover's clock stability, and the receiver's carrier tracking loop errors. Then, we solve for the rover's position using a weighted batch filter algorithm of the accumulated Doppler measurements.

In this analysis, we simulate the Lunar Pathfinder satellite in an Elliptical Lunar Frozen Orbit (ELFO). The noise for the Doppler shift measurements is modeled as a function of the carrier-to-noise ratio, obtained by modeling the transmitter and receiver antenna gain patterns. We also account for the frequency error of the rover's clock in the measurement model. In order to provide absolute localization for the Endurance rover, our approach estimates the mean and the 99 percentile of the absolute positioning error across 100 Monte Carlo realizations. We investigate these performance metrics under different degrees of clock stability and satellite ephemeris errors.

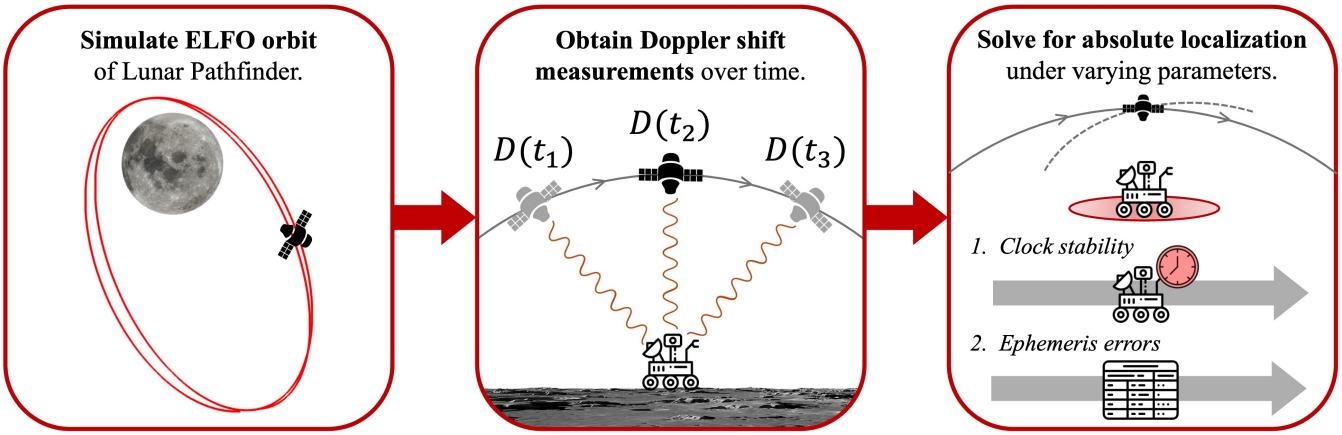

FIGURE 1: Flow chart of the proposed approach. First, we simulate the Lunar Pathfinder's orbital trajectory. Then, we obtain Doppler shift measurements that the Endurance rover will receive over time. Finally, we perform batch filter optimization to solve for the rover's absolute localization under different degrees of clock stability and ephemeris errors.

3. Key Contributions

A description of the new and innovative aspects of the paper are given below:

- To the best of the authors' knowledge, this paper is the first to employ a singular satellite with no navigation payload to localize a lunar surface user.
- We formulate a Doppler measurement error model to simulate realistic measurements from the Lunar Pathfinder communication signal, which accounts for effects including satellite ephemeris uncertainty, signal link budget, carrier tracking loop errors, and rover clock drift.
- Through Monte Carlo simulations, this work compares the trend in positioning errors over time when the rover is placed at different locations on the Moon.
- We perform sensitivity analyses on the convergence time to achieve sub-10-m level positioning under various degrees of clock stability and ephemeris error uncertainty.

4. Paper Organization

This paper is organized as follows: Section II outlines how the scenario is modeled, including Doppler shift measurement generation, the satellite orbit, transmitter and receiver antennae parameters, as well as PLL tracking error modeling. Section III describes the state estimation framework that refines the rover's position estimate from the Doppler shift observables. Section IV details the experimental set-up and Section V provides a discussion of the results. Finally, Section VI provides an overview of the accomplished tasks and summarizes the main findings of the paper.

II. SCENARIO MODELING

In this section, we address how we model the scenario presented in this paper, including the Doppler shift observables obtained from the Lunar Pathfinder, the satellite's orbit, and the communication signal transmitted from the satellite to the rover. We also detail the error models implemented in this work for satellite ephemeris and pseudorange rate measurements.

1. Doppler Shift Measurement Generation

Constrained to a single communication satellite, the Lunar Pathfinder, we utilize Doppler shift measurements as the observable for state estimation. Doppler shift measurements D are obtained by calculating the difference between the frequency of the signal emitted at the source f_{source} and the frequency of the signal that is received by the rover f_{received} due to the relative motion between the satellite and the rover. Given the Lunar Pathfinder satellite is not yet launched into lunar orbit, in this work, we simulate the Doppler shift measurement observables. In particular, the Doppler shift can be modeled as

$$D = f_{\text{received}} - f_{\text{source}} = -\frac{\dot{\rho}\, f_{\text{source}}}{c}, \tag{1}$$

where $c = 299\,792\,458\ \mathrm{m/s}$ is the speed of light and $\dot{\rho}$ is the pseudorange rate, or the apparent rate of change in the distance between the satellite and the rover. True range rate $\dot{\rho}_{\text{true}}$ is defined as the projection of the satellite's velocity onto the line of sight between the rover and the satellite (Misra and Enge, 2012):

$$\dot{\rho}_{\text{true}}^{(t)} = \mathbf{v}_{\mathbf{sat}}^{(t)} \cdot \frac{\mathbf{x}_{\mathbf{sat}}^{(t)} - \mathbf{x}_{\mathbf{rov}}}{\left\| \mathbf{x}_{\mathbf{sat}}^{(t)} - \mathbf{x}_{\mathbf{rov}} \right\|} \quad , \quad \mathbf{x}^{(t)} = [x \quad y \quad z]^\top \quad , \quad \mathbf{v}^{(t)} = [\dot{x} \quad \dot{y} \quad \dot{z}]^\top \tag{2}$$

where $\mathbf{x}_{\mathbf{sat}}^{(t)}$ and $\mathbf{v}_{\mathbf{sat}}^{(t)}$ represent the 3D satellite position and velocity, respectively, at time t and $\mathbf{x}_{\mathbf{rov}}$ represents the stationary rover position in the Moon Principal Axis frame (Folta et al., 2022). Pseudorange rate is a function of the observed measurements, which include errors due to the difference in reference frequencies between the source and the receiver.

2. Satellite Orbit Model

SSTL has designed the Lunar Pathfinder to orbit the Moon in an ELFO with orbital elements defined in the Moon Orbital Plane frame of reference as shown in Table 1 (SSTL, 2022). The orbital period as well as the periselene and aposelene altitudes are also provided. This orbital path was chosen by SSTL to ensure that there is long duration coverage of the Moon's southern hemisphere as well as long-term stability.

TABLE 1: The six Keplerian orbital elements as well as other orbital parameters of the Lunar Pathfinder's trajectory (SSTL, 2022)

Orbital Parameters	**Value**
Semi-major axis [km]	5740
Eccentricity	0.58
Inclination [°]	54.856
Right Ascension of the Ascending Node (RAAN) [°]	0
Argument of the Pericenter [°]	86.322
Mean Anomaly [°]	180
Periselene altitude [km]	673
Aposelene altitude [km]	7331
Orbital Period [hr]	10.84

3. Communication Signal Model

In this section, we discuss the structure of the Lunar Pathfinder's communication signal, the parameters of the satellite's transmitter and the rover's receiver, as well as the model for the carrier-to-noise density ratio C/N_0.

a) Lunar Pathfinder Communication Signal

The Lunar Pathfinder will provide both S-band and Ultra-High Frequency (UHF) communication channels to lunar users. The frequency for the downlink signals is set to be between 2025 and 2110 MHz. The rover's primary communication channel with the Lunar Pathfinder will be through S-band (Keane et al., 2022), so we use a midpoint value of 2050 MHz for our simulations.

b) Transmitter Antenna

Per Lunar Pathfinder's specification document (SSTL, 2022), the range of effective isotropic radiated power (EIRP) that the satellite will transmit to an autonomous rover is between 12 and 26.5 dB W. The S-band downlink signal is specified to be greater than 20.14 dB W at a half-power beamwidth (HPBW) angle of 7.1°. Thus in this work, we model the transmitting parabolic antenna gain pattern as having a 26.5 dB W power level at boresight, with a HPBW angle of 7.1°.

c) Receiver Antenna and Signal Tracking Loop

To communicate with the Lunar Pathfinder, the Endurance rover will be equipped with a 2-axis gimbaled 0.75-m S-band high gain antenna (Keane et al., 2022). The Endurance rover will have an antenna gain G_r of 22.5 dB and will track the Lunar Pathfinder as it moves in the sky. Keane et al. (2022) also specify that satellite tracking does not have to be very precise as a 3° tracking error will result in only a 0.5 dB gain loss. Therefore, we apply a conservative assumption that the receiver antenna gain G_r is 22 dB due to tracking error.

d) Carrier-to-Noise Density Modeling

Given the EIRP of the transmitter and the gain of the receiver antenna, we can determine the quality of the signal through the received carrier-to-noise density ratio C/N_0. The C/N_0 metric defines the pseudorange rate measurement error covariance, which will be elaborated on in Section II.5. The received C/N_0 is a function of the received isometric power P_r, the receiver's gain-to-noise-temperature ratio g/T, according to the following (in $\mathrm{dB\,Hz}$) (Delépaut et al., 2020; Misra and Enge, 2012):

$$C/N_0 = P_r + g/T - k, \tag{3}$$

where k is the Boltzmann constant, which is $-228.6\ \mathrm{dB\,W/(K\,Hz)}$. The received isometric power P_r uses EIRP as a function of the off-boresight angle β and the free space path loss, which is a function of the signal frequency f_S and the distance between transmitter and the receiver r.

$$P_r = EIRP(\beta) - 20\log_{10}\left(\frac{4\pi r f_S}{c}\right) \tag{4}$$

The receiver's gain-to-noise-temperature ratio g/T takes into account losses from the system temperatures. The equivalent noise temperature T_{eq} in Kelvin is a function of the receiver's system noise temperature T_{sys} and the noise figure from the receiver's low noise amplifier (LNA) NF_{LNA}, using a reference temperature of 290 K at the input of the LNA (Delépaut et al., 2020; Cortinovis et al., 2024). Equation 6 describes the formula for the equivalent noise temperature T_{eq} converted to its noise figure in dB. The receiver parameters in Equations 5 and 6 are described in Table 2.

$$g/T = G_r - T_{\text{eq}}, \tag{5}$$

$$T_{\text{eq}} = 10\log_{10}\left(T_{\text{sys}} + 290(10^{NF_{\text{LNA}}/10} - 1)\right) \tag{6}$$

TABLE 2: Parameters associated with the Endurance's rover receiver. These constants are used to obtain C/N_0 as shown in Equations 3 to 6. The system noise temperature and the noise figure are values for a lunar surface rover's S-band receiver (Audet et al., 2024).

Parameters	Symbol	Value
Gain of the receiver antenna [dB]	G_r	22.0
System noise temperature of the receiver antenna [K]	T_{sys}	113
Noise figure of the receiver's LNA [dB]	NF_{LNA}	1

4. Satellite Ephemeris Error Model

SSTL has not yet released the expected ephemeris errors of the Lunar Pathfinder. We assume that the rover will be able to downlink the ephemeris information through the communication signal, but the frequency at which the rover will have access to the updated information or the preciseness of the ephemeris is unknown. Given that a communication satellite relies less heavily on precise ephemeris knowledge as a navigation satellite would, we can infer that the ephemeris errors cited in the Lunar Relay Services Requirements Document for lunar navigation satellites will present a best-case scenario. According to the signal-in-space-error (SISE) requirements for a lunar relay position, navigation, and timing (PNT) satellite, the SISE position error is $13.43\ \mathrm{m}$ and the SISE velocity error is $1.2\ \mathrm{mm/s}$, both at 3σ (NASA, 2022). Due to the uncertainty in the Lunar Pathfinder's ephemeris knowledge, we conduct a sensitivity analysis on the positioning error with varying degrees of satellite ephemeris error in Section V.4. Thus, we provide the rover with erroneous satellite position and velocity states, and these ephemeris errors are added as white Gaussian noise to the satellite's true state:

$$\mathbf{x}_{\text{sat,noise}} = \mathbf{x}_{\text{sat,true}} + \epsilon_{\text{eph,pos}} \tag{7}$$

$$\mathbf{v}_{\text{sat,noise}} = \mathbf{v}_{\text{sat,true}} + \epsilon_{\text{eph,vel}}, \tag{8}$$

where the satellite position and velocity errors are sampled as $\epsilon_{\text{eph,pos}} \sim \mathcal{N}(0, \sigma^2_{\text{eph,pos}_{xyz}} I_3)$ and $\epsilon_{\text{eph,vel}} \sim \mathcal{N}(0, \sigma^2_{\text{eph,vel}_{xyz}} I_3)$, and where I_3 represents the 3×3 identity matrix.

5. Pseudorange Rate Measurement Error Model

Outside of ephemeris errors, we must account for uncertainty in the pseudorange rate measurements. In this section, we discuss how we model the noise due to carrier tracking and clock frequency errors.

a) Carrier Tracking

For this pseudorange rate model, we assume that one of the main sources of error is due to carrier tracking. We predict that the receiver will track the incoming carrier frequency using a phase locked loop (PLL) to obtain the Doppler frequency measurement. The thermal noise of the PLL is oftentimes the largest source of error in tracking the carrier frequency (Kaplan and Hegarty, 2017). The PLL thermal noise σ_{PLL} is given in Equation 9 (Kaplan and Hegarty, 2017; Borio et al., 2011). The constants used in Equation 9 are detailed in Table 3.

$$\sigma_{\text{PLL}} = \frac{c}{2\pi f_S T}\sqrt{\frac{B_{\text{PLL}}}{C/N_0}\left(1+\frac{1}{2\,T\,C/N_0}\right)} \tag{9}$$

TABLE 3: Parameters for PLL tracking. These are commonly used values for PLL error modeling (Nardin et al., 2023; Audet et al., 2024; Kaplan and Hegarty, 2017).

Parameters	Symbol	Value
PLL bandwidth [Hz]	B_{PLL}	10
Coherent time integration [s]	T	0.02

b) Clock Stability

Another contributor to the measurement error is the frequency error of the rover's clock. The frequency error σ_{clock} can be described using the following equations (O'Dea et al., 2019).

$$\sigma_{\text{clock}} = c \cdot \sigma_f \tag{10}$$

$$\sigma_f^2 = \frac{h_0}{2\tau} + 4h_{-1} + \frac{8}{3}\pi^2\tau h_{-2} \tag{11}$$

where σ_f is the deviation in the rover clock's fractional frequency (Krawinkel and Schön, 2016). h_0, h_{-1}, and h_{-2} are the power spectral density (PSD) coefficients that describe the stability of the clock and τ is the measurement sampling time. We only need to consider the rover clock's frequency error because the satellite clock's frequency error is encapsulated by the SISE, which is accounted for in the satellite ephemeris error model.

In this work, we consider four clocks for the rover of various sizes, weights, and power consumption (SWaP). Table 4 details the time deviation (TDEV) values per day and the PSD coefficients of the considered rover clocks in increasing SWaP. As expected, the lower SWaP clocks have larger time deviation values per day and therefore, larger clock drift (note that clock drift is the time deviation per second). We investigate the performance all four clocks in our clock sensitivity study in Section V.3.

TABLE 4: SWaP values, time deviation (TDEV) values per day, and the PSD coefficients for the rover clock candidates (Schmittberger and Scherer, 2020; Bhamidipati et al., 2022). The Excelitas RAFS clock is stable enough that the contributions from the h_{-1} and h_{-2} coefficients are considered to be negligible.

Clock Type	Size [cm^3]	Weight [kg]	Power [W]	TDEV per day [µs]	h_0 [s^2/s]	h_{-1} [s^2/s^2]	h_{-2} [s/s^2]
Microchip CSAC	17	0.035	0.12	1.5	1.3×10^{-20}	1.0×10^{-24}	3.7×10^{-29}
Microchip MAC	50	0.086	5	0.17	4.7×10^{-22}	1.2×10^{-25}	1.7×10^{-30}
SRS PRS 10	155	0.6	14.4	7.0×10^{-2}	1.3×10^{-22}	2.3×10^{-26}	3.3×10^{-31}
Excelitas RAFS	1645	6.35	39	4.8×10^{-3}	8.0×10^{-27}	–	–

c) Total Measurement Error Model

In summary, we model the pseudorange rate variance as the sum of the variances of the thermal noise of the PLL and the rover clock's frequency error:

$$\sigma_{\dot{\rho}}^2 = \sigma_{\text{PLL}}^2 + \sigma_{\text{clock}}^2 \tag{12}$$

The error term is represented as a zero-mean white Gaussian noise with variance $\sigma_{\dot{\rho}}^2$. The rover's observed measurements are also offset by how much the satellite's and rover's clocks have drifted with respect to one another. The observed, or noisy, pseudorange rate model is as follows:

$$\dot{\rho}_{\text{obs}} = \dot{\rho}_{\text{true}} + c\left(\dot{\delta t}_{\text{sat}} - \dot{\delta t}_{\text{rov}}\right) + \epsilon_{\dot{\rho}} \ , \quad \epsilon_{\dot{\rho}} \sim \mathcal{N}(0, \sigma_{\dot{\rho}}^2) \tag{13}$$

where $\dot{\delta t}_{\text{sat}}$ and $\dot{\delta t}_{\text{rov}}$ are the satellite's and rover's clock drifts, respectively. In this work, we assume that the satellite's clock is stable and the rover's clock drift is constant throughout the measurement window.

The total measurement error is defined as

$$\sigma_{\text{tot}}^2 = \sigma_{\text{eph,vel}}^2 + \sigma_{\dot{\rho}}^2 \tag{14}$$

Equation 14 is used for a weighting matrix in the measurement filtering to prioritize the measurements with less variance. The implementation of Equation 14 is described in Section III.

III. STATE ESTIMATION FRAMEWORK

We now address the state estimation framework implemented to resolve the rover state with Doppler observables from the Lunar Pathfinder communication signal. In a traditional scenario for localizing a ground user via satellites, an Extended Kalman Filter (EKF) is commonly used as the nonlinear state estimation framework because it updates the rover's position estimate with each time step, making it a computationally efficient state estimation algorithm. However, in our single-satellite scenario, we can only obtain one measurement at each time step, necessitating the accumulation of these measurements over time. Therefore, for our state estimation framework, we consider a weighted batch filter because it can process multiple measurements over time, drastically improving our measurement geometry in comparison to the EKF. In this section, we detail the formulation of the weighted batch filter for processing pseudorange rate measurements over time while accounting for clock drift.

1. Weighted Batch Filter Formulation

The weighted batch filter first accumulates observed pseudorange rate measurements over time to diversify the measurement geometry. With each iteration k of the batch filter, the batch of measurements that the filter processes increases in size since we retain all previous measurements in this framework. Let us define $\mathbf{y}$ to be the stack of N measurements in a given batch of measurements that are accumulated over time.

$$\mathbf{y} = \begin{bmatrix} \dot{\rho}_{\text{obs},1} & \dot{\rho}_{\text{obs},2} & \cdots & \dot{\rho}_{\text{obs},N} \end{bmatrix}^\top \tag{15}$$

For each batch of measurements, we predict the pseudorange rate observables that the rover expects to obtain at time t, given that the rover will have noisy satellite knowledge. The expected pseudorange rate observables $\hat{\dot{\rho}}_{\text{obs}}$ is of similar form as Equation 13 and is defined below. Note that the expected measurements incorporate the rover's state estimate $\hat{\mathbf{x}}$ and the noisy satellite's state. We also set the satellite's clock drift to be zero because we assume that the clock onboard the Lunar Pathfinder is stable. The stack of expected measurements $\hat{\dot{\rho}}_{\text{obs}}$ for each filter iteration k is defined as $\hat{\mathbf{y}}_k$.

$$\hat{\dot{\rho}}_{\text{obs}}^{(t)} = \mathbf{v}_{\textbf{sat,noise}}^{(t)} \cdot \frac{\mathbf{x}_{\textbf{sat,noise}}^{(t)} - \hat{\mathbf{x}}}{\left\| \mathbf{x}_{\textbf{sat,noise}}^{(t)} - \hat{\mathbf{x}} \right\|} + c\left(\dot{\delta t}_{\text{sat}} - \dot{\delta t}_{\text{rov}}\right) \tag{16}$$

In order to refine the rover's state estimate to $\hat{\mathbf{x}}_{k+1}$, we must also refine the batch of expected pseudorange rate measurements to $\hat{\mathbf{y}}_{k+1}$. The expected pseudorange rate model as defined in Equation 16 is nonlinear, so we obtain $\hat{\mathbf{y}}_{k+1}$ by performing a first order Taylor series approximation about the rover's current state estimate $\hat{\mathbf{x}}_k$.

$$\hat{\mathbf{y}}_{k+1} = \hat{\mathbf{y}}_k + \frac{\partial \hat{\mathbf{y}}_k}{\partial \hat{\mathbf{x}}_k}(\hat{\mathbf{x}}_{k+1} - \hat{\mathbf{x}}_k) \tag{17}$$

$$= \hat{\mathbf{y}}_k + \mathbf{H}_k \delta \mathbf{x} \tag{18}$$

Above, we define $\delta \mathbf{x}$ as the difference in the current and updated rover's state estimate. The first derivative of the expected pseudorange rate measurement stack $\hat{\mathbf{y}}_k$ with respect to the current rover's state estimate $\hat{\mathbf{x}}_k$ is defined as the measurement

Jacobian matrix $\mathbf{H}_k$:

$$\mathbf{H}_k = \begin{bmatrix} \frac{\partial \hat{\hat{\rho}}_{\text{obs},1}}{\partial \hat{\mathbf{x}}_k} & \frac{\partial \hat{\hat{\rho}}_{\text{obs},2}}{\partial \hat{\mathbf{x}}_k} & \cdots & \frac{\partial \hat{\hat{\rho}}_{\text{obs},N}}{\partial \hat{\mathbf{x}}_k} \end{bmatrix}^\top \in \mathbb{R}^{N\times 4}\,, \tag{19}$$

$$\frac{\partial \hat{\hat{\rho}}_{\text{obs},t}}{\partial \hat{\mathbf{x}}_k} = \begin{bmatrix} \frac{\partial \hat{\hat{\rho}}_{\text{obs},t}}{\partial x_k} & \frac{\partial \hat{\hat{\rho}}_{\text{obs},t}}{\partial y_k} & \frac{\partial \hat{\hat{\rho}}_{\text{obs},t}}{\partial z_k} & 1 \end{bmatrix} \quad , \quad \hat{\mathbf{x}}_k = \begin{bmatrix} x_k & y_k & z_k & c\cdot \dot{\delta} t_k \end{bmatrix}^\top \tag{20}$$

When refining the rover's state estimate, we must take into account the rover's clock drift since it contributes to the rover's expected pseudorange rate measurements. Therefore, in the measurement Jacobian, we consider the rover's clock drift (multiplied by the speed of light) as the fourth element of the rover's state. Recall that we assume that the rover's clock drift is constant throughout the measurement window, which results in the fourth column of the Jacobian to be $\mathbf{1}_{N\times 1}$. As a note, the fourth element of the rover's state is removed from $\hat{\mathbf{x}}$ in Equation 16 to maintain the same matrix size as the satellite's state and is instead added separately in the second term of the equation.

Ultimately, the rover's updated position estimate $\hat{\mathbf{x}}_{k+1}$ is obtained by minimizing the difference between the observed pseudorange rate measurements and the expected pseudorange rate measurements that we have refined, as seen in Equation 21. We define this difference to be the measurement residual $\delta\mathbf{y}$. By utilizing the Taylor series approximation from Equation 18, the cost function to minimize is shown in Equation 22, which has a closed-form solution as shown in Equation 23.

$$J = \|\mathbf{y} - \hat{\mathbf{y}}_{k+1}\|^2_{\mathbf{W}} \tag{21}$$

$$= \|\delta\mathbf{y} - \mathbf{H}_k\delta\mathbf{x}\|^2_{\mathbf{W}} \tag{22}$$

$$\delta\mathbf{x} = \left(\mathbf{H}_k^\top \mathbf{W}\mathbf{H}_k\right)^{-1}\mathbf{H}_k^\top\mathbf{W}\delta\mathbf{y} \tag{23}$$

We use a weighting matrix $\mathbf{W}$ in the measurement filtering to prioritize the measurements with less variance. The weighting matrix $\mathbf{W}$ is a function of the total measurement error as defined in Equation 14.

$$\mathbf{W} = \text{diag}(\sigma^{-2}_{\text{tot},1}\ ,\ \ldots\ ,\ \sigma^{-2}_{\text{tot,N}}) \tag{24}$$

For each batch of measurements, we iteratively update $\delta\mathbf{x}$ (and thus $\hat{\mathbf{x}}$) until $\delta\mathbf{x}$ is negligibly small. This iterative process, the Gauss-Newton method, is outlined in Algorithm 1. The `simulate_pseudorange_rate()` function in Algorithm 1 outputs the expected measurement stack and the Jacobian as defined in Equations 16 and 19, respectively. The updated state estimate is stored after each batch is processed. With each new batch of measurements, the rover's state estimate is re-initialized and refined once again through the batch filter. When the satellite is not visible the rover, measurements cannot be collected. During this occultation period, the rover's current state estimate is not updated.

2. Filter Initialization

We modify the initialization of the Gauss-Newton method by embedding prior knowledge about the rover's initial position estimate in the algorithm. In other words, we augment $\mathbf{H}_k$ and $\delta\mathbf{y}$ by treating the residual between the initial estimate $\hat{\mathbf{x}}_0$ and the current estimate $\hat{\mathbf{x}}_k$ as a measurement. The uncertainty of the initial estimate is also embedded in the weighting matrix $\mathbf{W}$. The augmentations to $\mathbf{H}_k$, $\delta\mathbf{y}$, and $\mathbf{W}$ can be found in lines 5, 6, and 7 of Algorithm 1, respectively.

This modification ensures that there is no significant divergence from the rover's true state early in the simulation. When the initial position estimate is not embedded into the algorithm, we observe a spike in the rover's positioning error. This augmentation helps maintain a stable estimate until there are enough measurements to resolve the rover's state at a finer accuracy.

IV. EXPERIMENTAL SET-UP

In this section, we outline the experimental set-up to evaluate the feasibility and performance of single-satellite lunar surface state estimation with only Doppler shift observables. We discuss the location of the rover on the Moon where state estimation is performed, as well as the simulation parameters for the Monte Carlo simulations.

1. Initialized Rover Position

According to the Endurance Mission Concept Study Report (Keane et al., 2022), there are two implementation options being considered for the Endurance mission: (1) Endurance-R, where the rover will rendezvous with a Earth Return Vehicle to return the samples and (2) Endurance-A, where the rover will meet with the Artemis astronauts who will then bring the samples back to Earth. Endurance-R will begin its path at the Poincaré Q basin and end at the Apollo peak ring, while Endurance-A will

Algorithm 1 Weighted Gauss-Newton Method for Rover Localization

Require: Initial rover position estimate $\hat{\mathbf{x}}_0$, observed pseudorange rate measurements $\mathbf{y}$, rover's knowledge of satellite position $\mathbf{x}_{\text{sat,noise}}$ and velocity $\mathbf{v}_{\text{sat,noise}}$, measurement time t
Ensure: Final rover position estimate $\hat{\mathbf{x}}$

for each batch of measurements at time t **do**
  if satellite is visible **then**
    while $\|\delta\mathbf{x}\| > 10^{-9}$ **do**
      $[\hat{\mathbf{y}}_k, \mathbf{H}_k] \leftarrow \texttt{simulate\_pseudorange\_rate}(\mathbf{x}_{\text{sat,noise}}, \mathbf{v}_{\text{sat,noise}}, \hat{\mathbf{x}})$
      $\mathbf{H}_k \leftarrow [\mathbf{I}_{3\times 3}\,,\, \mathbf{0}_{3\times 1}\,;\, \mathbf{H}_k]$
      $\delta\mathbf{y} \leftarrow [\hat{\mathbf{x}}_0 - \hat{\mathbf{x}}\,;\, \mathbf{y} - \hat{\mathbf{y}}_k]$
      $\mathbf{W} \leftarrow \text{diag}(\sigma_{\text{pos}}^{-2}\,,\, \sigma_{\text{pos}}^{-2}\,,\, \sigma_{\text{pos}}^{-2}\,,\, \sigma_{\text{tot,1}}^{-2}\,,\, \ldots\,,\, \sigma_{\text{tot,N}}^{-2})$
      $\delta\mathbf{x} \leftarrow (\mathbf{H}_k^T\mathbf{W}\mathbf{H}_k)^{-1}\mathbf{H}_k^T\mathbf{W}\delta\mathbf{y}$
      $\hat{\mathbf{x}} \leftarrow \hat{\mathbf{x}} + \delta\mathbf{x}$
    end while
  end if
end for
return $\hat{\mathbf{x}}$

start in the central SPA and reunite with the astronauts at the Artemis Basecamp. For this study, we have selected three key locations–Poincaré Q, Apollo peak ring, and the Artemis Basecamp–as shown in Figure 2, since these locations are sufficiently spatially distributed with respect to each other in the SPA basin. Cortinovis et al. (2024) also conduct their analyses at these locations. Table 5 details the latitude and longitude coordinates of the selected waypoints.

Upon landing on the surface of the Moon, the rover will have good initial state estimation knowledge via manual human-in-the-loop map comparison. Therefore, the initial positioning error is on the order of 100 m for this study. The initial state estimate is randomly sampled from a Gaussian normal distribution such that $\hat{\mathbf{x}}_0 \sim \mathcal{N}(\mathbf{0}, \text{diag}[100^2, 100^2, 100^2])$ m.

2. Simulation Parameters

The starting epoch to determine the Lunar Pathfinder's orbit with respect to the Moon is set to 2030 October 1, 00:00 UTC. We consider two orbital periods, or about 22 hours, for our simulation time unless otherwise specified. Measurements are

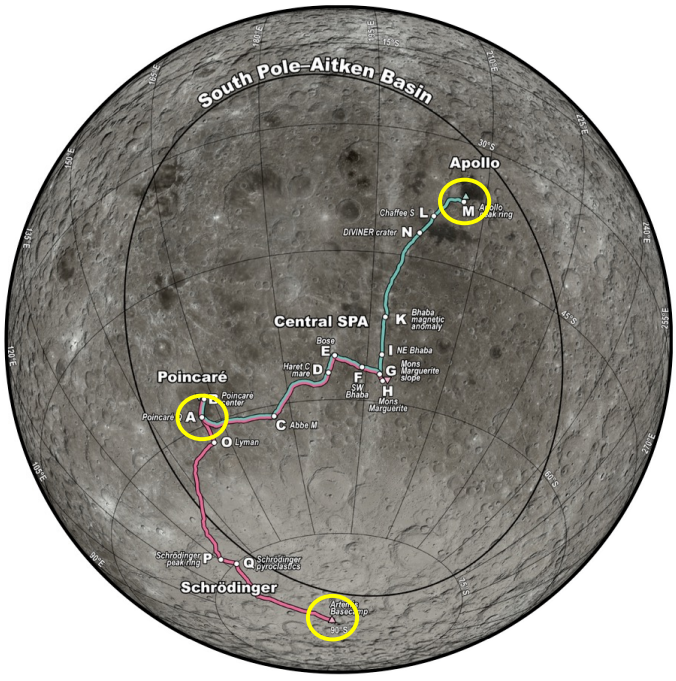

FIGURE 2: Map of Endurance's path with chosen waypoints circled in yellow. Figure adapted from Keane et al. (2022).

TABLE 5: Latitude and longitude of the selected waypoints. Keane et al. (2022) specify the coordinates for Poincaré Q and the Apollo peak ring. Since the exact location of the Artemis Basecamp is not yet finalized, we have approximated its location to be at the South Pole.

Location	Latitude [°]	Longitude [°]
Poincaré Q	−59.12448	161.05104
Apollo Peak Ring	−37.7115	−153.0430
Artemis Basecamp	−90	0

sampled at 1 Hz and the batch filter provides a new update of the rover's state every 180 seconds. Note that no measurements are acquired when the Lunar Pathfinder satellite is not visible to the rover. Metrics that define signal availability are described in Section V.1. Since we perform random sampling of the initial position estimate, satellite ephemeris errors, and the Doppler measurement errors, we conduct 100 Monte Carlo realizations of the batch filter per location of interest.

V. ANALYSIS AND RESULTS

In this section, we first discuss the availability of the communication signal at each location considered. Then, we address the performance of the state estimation framework at each location with nominal error modeling. In this study, we investigate the time for the absolute positioning error to converge to below 10 m, which is the global localization error requirement for the Endurance mission (Cauligi et al., 2023). Absolute positioning error of the rover is defined as the L_2 norm of the difference between the true and the estimated position. We consider the mean and the 99 percentile of the absolute positioning error across all of the Monte Carlo realizations as our performance metrics. Finally, we discuss the effects of different degrees of clock stability and satellite ephemeris errors on achieving the desired state estimation accuracy.

1. Signal Availability

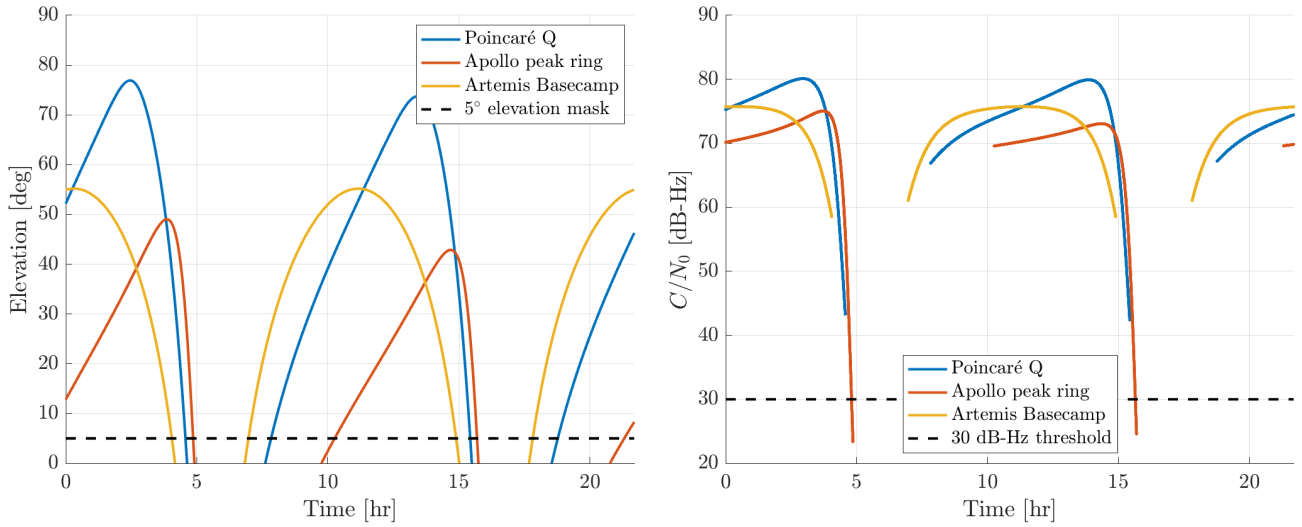

FIGURE 3: [Left] Elevation angle of the Lunar Pathfinder and [right] received carrier-to-noise density ratio C/N_0 (given that the satellite is visible) over two orbital periods for each of the three lunar sites considered.

The design of the Lunar Pathfinder's ELFO allows for favorable coverage of the SPA region. Figure 3 presents the received C/N_0 and the elevation mask over two orbital periods. Contrary to intuition, the received C/N_0 is highest when the satellite is at its maximum elevation (i.e., when the satellite is farthest from the rover). We would expect C/N_0 to reach a minimum at the highest elevation point due to increased free-space path loss. However, this assumption only holds with accurate antenna pointing. In this scenario, the Lunar Pathfinder is unable to track the rover perfectly since it simultaneously services multiple lunar assets. As a result, the directionality of the transmitting antenna significantly influences the received C/N_0. When the satellite is directly overhead, it points most accurately toward the rover, leading to a higher C/N_0 despite the larger distance.

We consider an elevation mask of 5° for satellite visibility, and we define the signal to be available when the received signal strength is larger than 30 dB Hz (as is done in Nardin et al. (2023) and Melman et al. (2022)). Based on the respective thresholds,

the 5° elevation mask is the limiting factor for satellite visibility in comparison to the $30\ \mathrm{dB\,Hz}$ signal strength threshold. The regions where the satellite is not visible to the rover are shown as gray occultation zones in later figures.

Table 6 provides the total time duration where the satellite signal is unavailable, either due to insufficient received C/N_0 or lack of satellite visibility. The total occultation period for each location is the union of the two metrics (i.e., when $C/N_0 < 30\ \mathrm{dB\,Hz}$ or when elevation $< 5^\circ$). The Artemis Basecamp location has the shortest occultation period while the Apollo peak ring has the longest occultation period due to the elevation mask. Since the Artemis Basecamp is located exactly at the South Pole, the rover's position is symmetric relative to the Lunar Pathfinder as seen in the elevation plot in Figure 3. This results in no change in the occultation period between the first and second orbits for the Artemis Basecamp location. In contrast, for the Poincaré Q and Apollo peak ring locations, the occultation periods slightly increase between the first and second orbits due to the satellite's relative motion.

Cortinovis et al. (2024) also use the same metrics for signal availability. However, because they assume that the satellite is equipped with a navigation payload, they model their transmitter antenna according to the Lunar Communications Relay and Navigation Systems (LCRNS) requirements, resulting in smaller C/N_0 values than we observe with the transmitter parameters used in this study. Thus, our modeling of a lunar satellite with a communication antenna results in longer periods of signal availability in comparison to a lunar satellite with a navigation antenna (Cortinovis et al., 2024).

TABLE 6: The length of time, in hours, where the elevation mask is less than 5° and the received C/N_0 is less than $30\ \mathrm{dB\,Hz}$ (given that the satellite is visible) for each key location. The total length of the occultation period, considering both metrics, is also provided. Each cell displays the length of time of the occultation period corresponding to the first and the second orbit.

Location	**Length of the first and second occultation periods**					
	Elevation $< 5^\circ$		$C/N_0 < 30\ \mathrm{dB\,Hz}$		Total	
	First	Second	First	Second	First	Second
Poincaré Q	$3.28\ \mathrm{hr}$	$3.36\ \mathrm{hr}$	$0.00\ \mathrm{hr}$	$0.00\ \mathrm{hr}$	$3.28\ \mathrm{hr}$	$3.36\ \mathrm{hr}$
Apollo Peak Ring	$5.41\ \mathrm{hr}$	$5.63\ \mathrm{hr}$	$0.05\ \mathrm{hr}$	$0.05\ \mathrm{hr}$	$5.46\ \mathrm{hr}$	$5.68\ \mathrm{hr}$
Artemis Basecamp	$2.92\ \mathrm{hr}$	$2.92\ \mathrm{hr}$	$0.00\ \mathrm{hr}$	$0.00\ \mathrm{hr}$	$2.92\ \mathrm{hr}$	$2.92\ \mathrm{hr}$

Figure 4 illustrates the behavior of the Doppler shift measurements. Positive Doppler measurements signify that the Lunar Pathfinder is approaching its peak elevation over the stationary Endurance rover, and negative measurements indicate that the satellite is receding. In the sub-figure on the right, the Lunar Pathfinder is traversing its path in the clockwise direction. The blue point in the figure marks the point in the satellite's path where the mean anomaly is 180°. At time $t = 0$ in the left sub-figure, the satellite is at the blue point in the right sub-figure. When the satellite recedes away from the blue point, it results in a negative Doppler shift until it enters the first occultation zone. Once the satellite re-enters the rover's line of sight, the satellite approaches peak elevation, resulting in a positive Doppler shift until it reaches zero Doppler shift at the blue point. For our state estimation experiments, we begin measurement collection once the satellite is visible to the rover (as indicated by the black arrow in the figure) to maximize the time for the rover to refine its position estimate before hitting an occultation zone.

2. State Estimation Performance

Using the weighted batch filter framework, we refine the rover's position estimate over time for each of the three locations. The mean μ, range of 1σ values, and the 99% error of the position estimation for 100 Monte Carlo realizations are shown in Figure 5. The figure also marks the occultation zones and the $10\ \mathrm{m}$ threshold for each location. All three plots are simulated under the assumption that the rover is equipped with an SRS PRS 10 clock and that the ephemeris errors are $4.48\ \mathrm{m}$ in position and $0.40\ \mathrm{mm/s}$ in velocity. (The justification for this ephemeris error is described in Section V.4.) Table 7 summarizes the time it takes for the mean μ and the 99% error of 100 Monte Carlo realizations to achieve sub-10-m accuracy.

TABLE 7: The time, in hours, for the mean and 99% error of 100 Monte Carlo runs to converge below the $10\ \mathrm{m}$ threshold for each location.

Location	**Time to reach $\leq$ 10 m**	
	Mean [hr]	99% error [hr]
Poincaré Q	11.6	16.0
Apollo Peak Ring	11.5	14.4
Artemis Basecamp	7.5	16.4

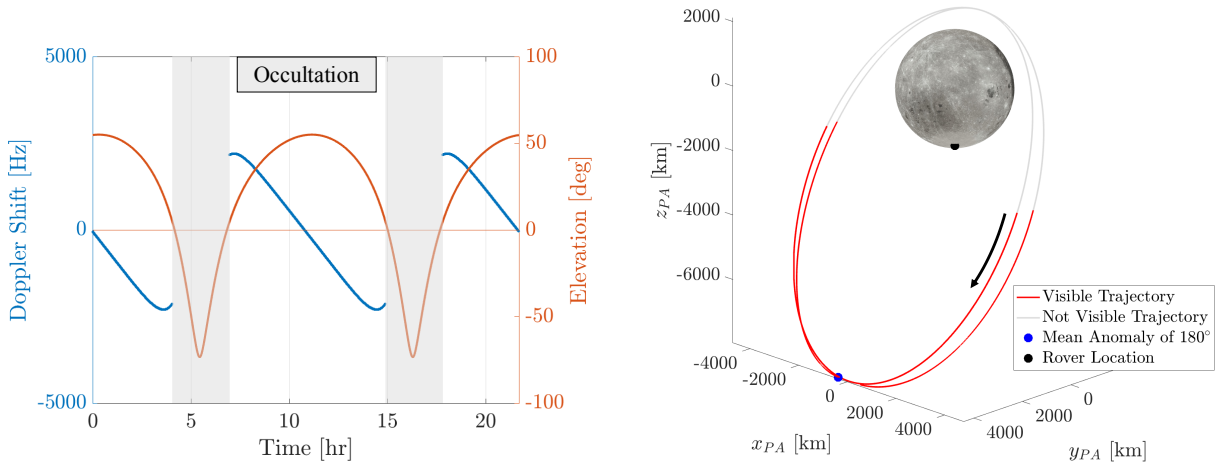

FIGURE 4: [Left] Doppler shift and elevation and [right] trajectory of the Lunar Pathfinder over two orbital periods. The rover's location is set to be at the Artemis Basecamp. Time $t = 0$ in the left sub-plot corresponds to the time when the satellite is located at the blue point in the right sub-plot. Measurement collection for state estimation begins once the satellite is visible to the rover, as shown by the black arrow.

From Figure 5, we observe that the mean position error μ reaches sub-10-m level accuracy within the first 12 hours for the Poincaré Q and the Apollo peak ring locations, and within 8 hours for the Artemis Basecamp location. The 99% error converges to 10 m within the first two orbital periods for all three locations. The mean positioning error for the Artemis Basecamp location

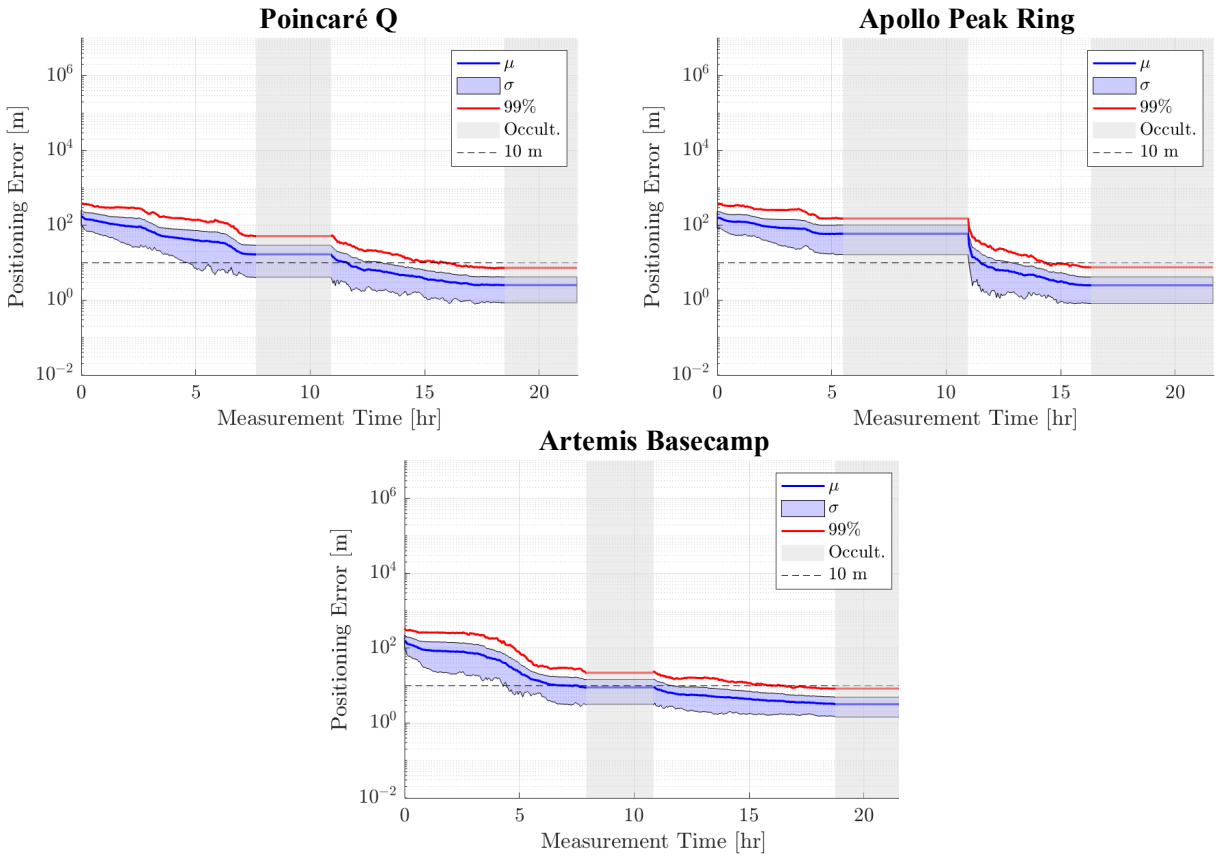

FIGURE 5: Positioning error over two orbital periods at three different locations. These plots are simulated with satellite ephemeris errors according to the LCRNS's SISE specification and with the assumption that the rover is equipped with an SRS PRS 10 clock.

is the only metric that is able to converge to below 10 m before the first occultation period. For an autonomous rover such as Endurance, the mean contact time per day that Lunar Pathfinder will be providing communication services is 529 minutes, or 8.82 hours (SSTL, 2022). While the exact periods of time when the Lunar Pathfinder will provide communication services is not yet specified, according to our analysis, we find that the rover, on average, will be able to localize itself within the desired accuracy within 8.82 hours only when the rover is located in the more southern regions of the rover's path. Otherwise, the rover will require a larger measurement window to successfully localize.

Despite having the shortest occultation period, the Artemis Basecamp location resulted in the largest 99% positioning error in comparison to the other locations as seen in Table 7. Since the Artemis Basecamp is located exactly at the South Pole, the diversity of measurements between the first visibility zone to the second visibility zone is minimal. Therefore, the rover's state estimate is slow to improve after the first occultation zone when the rover is located at the Artemis Basecamp.

Overall, we observe a plateau in positioning error in the first 3 to 4 hours for all three locations. This plateauing behavior occurs because we embed prior knowledge about the rover's initial position estimate, as described in Section III.2. In the first few hours, the rover does not have sufficient measurement diversity to refine the rover's state estimate to a finer accuracy. We find that the 99% error in this study takes approximately 10.7 to 13.6 hours longer to converge than in the study using two-way ranging measurements with the weighted batch filter (Cortinovis et al., 2024). The convergence window of the 99% error in this study includes an entire occultation period, which adds an additional 2.92 to 5.68 hours during which the estimate is not being refined. However, it is essential to note that a comprehensive comparison of this study and that of Cortinovis et al. (2024) is limited by the differences in modeling the measurement and ephemeris errors. Furthermore, we take into account noise due to the rover's onboard clock, which is not assessed in the study done by Cortinovis et al. (2024) since their model utilized two-way measurements.

3. Sensitivity Study on Clock Stability

NASA has not yet specified the type of clock that the Endurance rover will carry onboard. To help inform this decision, we conduct a sensitivity study to evaluate various clock candidates for the specific use case of localizing the rover. Table 4 details the SWaPs, TDEVs per day, and the PSD coefficients for the four rover clock candidates we consider in this study. We evaluate the time to achieve sub-10-m accuracy for each of the rover clocks and have summarized the performance metrics in Table 8.

TABLE 8: The time, in hours, for the mean and 99% error of 100 Monte Carlo runs to converge below the 10 m threshold for each of the different clock types (listed in the order of increasing SWaP). The rover is located in the South Pole for these simulations, and we use the LCRNS's SISE values to describe its ephemeris knowledge.

Clock Type	**Time to reach $\leq$ 10 m**	
	Mean [hr]	99% error [hr]
Microchip CSAC	50.1	Did not converge within 65 hrs
Microchip MAC	11.2	26.7
SRS PRS 10	7.5	16.4
Excelitas RAFS	4.9	11.1

Out of the SWaP metrics, we consider weight as being the most critical factor to minimize because of the cost to deploy heavy objects to the Moon. Therefore, we conduct a trade off analysis between clock stability and weight. Figure 6 displays a plot of the mean convergence time to achieve sub-10-m accuracy for the clock candidates, with the weights plotted on the y-axis. As expected, the heavier clocks (which correlate to less clock drift) take less time to convergence in comparison to the lighter clocks. The smallest clock that we consider–the Microchip CSAC–requires 5 orbital periods for the mean time to converge. The 99% error is unable to converge within 6 orbital periods for the Microchip CSAC. Therefore, we do not recommend the Microchip CSAC for single-satellite localization.

The most stable clock–the Excelitas RAFS–is able to converge in 4.9 hours. If clock weight and performance time both need to be minimized with equal magnitude, we recommend the SRS PRS 10 and the Microchip MAC clocks for the Endurance rover since they are less than 1 kg and converge within 1 to 2 orbital periods. However, if fast localization is more critical than additional weight on the rover, we recommend the Excelitas RAFS.

4. Sensitivity Study on Satellite Ephemeris Errors

Due to the uncertainty of the Lunar Pathfinder's ephemeris knowledge, we examine the effects of varying degrees of satellite ephemeris errors on achieving the desired position estimation accuracy. We consider the lowest satellite ephemeris errors to be

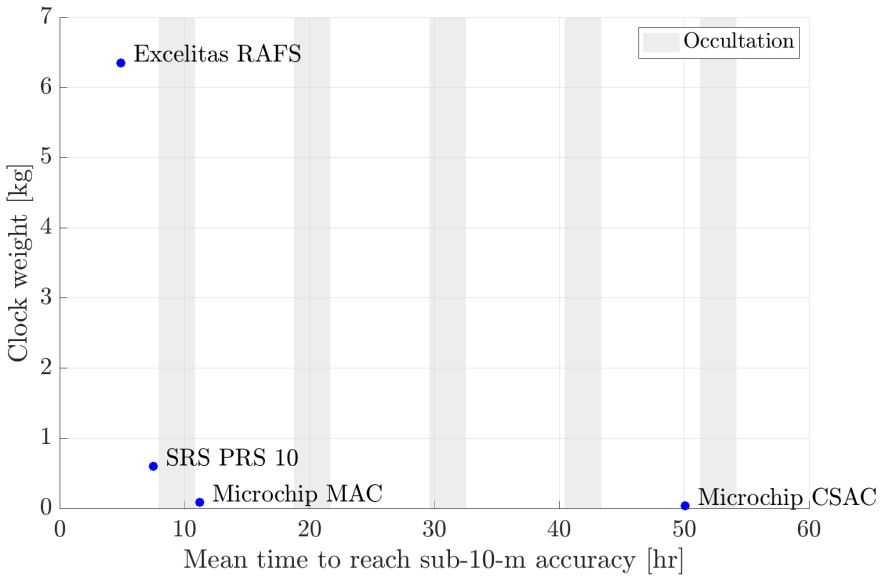

FIGURE 6: Mean time to reach sub-10-m accuracy for the four clock candidates, with their respective clock weights plotted on the y-axis. This study is done under the assumption that the rover is located at the Artemis Basecamp and is using the LCRNS's SISE values to describe its ephemeris knowledge.

those cited in the Lunar Relay Services Requirements Document (SRD) for lunar navigation satellites, which are $\sigma_{\text{eph,pos}} = 4.48\,\text{m}$ and $\sigma_{\text{eph,vel}} = 0.40\ \text{mm/s}$ (NASA, 2022). For our sensitivity analysis, we linearly inflate ephemeris errors ranging from 10.00 to $50.00\ \text{m}$ in position to 1.00 to $5.00\ \text{mm/s}$ in velocity, as seen in Figure 7.

We observe that the positioning error converges to below the $10\ \text{m}$ threshold in roughly the same amount of time for the lowest ephemeris errors and for $\sigma_{\text{eph,pos}} = 10.00\ \text{m}$ and $\sigma_{\text{eph,vel}} = 1.00\ \text{mm/s}$. However, for larger ephemeris errors, the 99% positioning error is unable to converge within two orbital periods, resulting in an additional 2.92 hours to the time for convergence. Based on this sensitivity study, we recommend that the Lunar Pathfinder's ephemeris errors remain below $20.00\ \text{m}$ in position and $2.00\ \text{mm/s}$ in velocity.

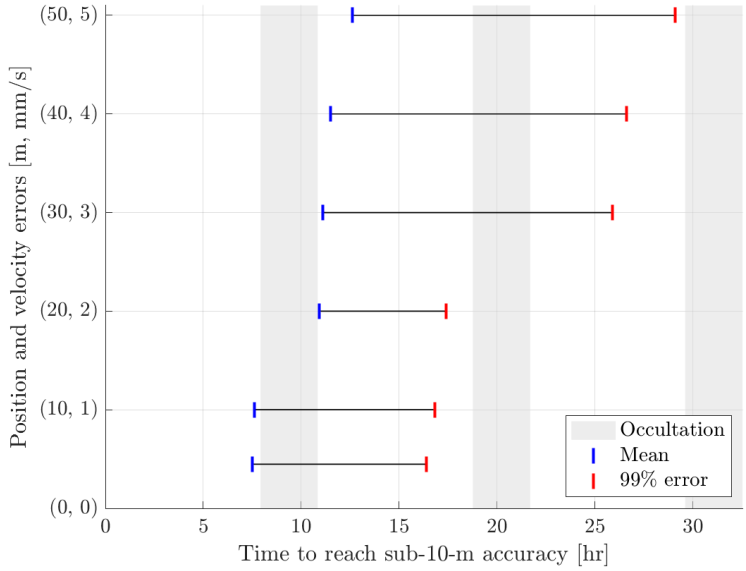

FIGURE 7: Time for the mean and 99 percentile of MC runs to converge to below $10\ \text{m}$ for different ephemeris errors in position [m] and velocity [mm/s]. This study is assumes that the rover is located at the Artemis Basecamp and is equipped with an SRS PRS 10 clock.

VI. CONCLUSIONS

We present a localization framework for the NASA JPL Endurance rover using only the downlinked communication signals from a single satellite, the SSTL Lunar Pathfinder, with no navigation payload. We design a weighted batch filter framework, which accumulates Doppler shift measurements and refines the position estimate of the stationary rover. For our analysis, we formulate a Doppler measurement model to simulate realistic measurement errors from the Lunar Pathfinder's communication signal, which accounts for the rover's clock drift, the satellite ephemeris errors, and the carrier tracking loop errors. We further model the signal link budget from the Lunar Pathfinder satellite to the Endurance rover while incorporating models of the satellite and receiver antennae, according to the available specifications of the respective missions. Through our analysis, we find that the mean and 99% positioning error of 100 Monte Carlo realizations were able to localize the rover with the desired sub-10-m accuracy within two orbital periods. We also perform sensitivity studies on the rover's clock type and ephemeris knowledge to better inform design decisions for the rover. Therefore, we demonstrate that utilizing opportunistic Doppler shift measurements as the only navigation observable is a feasible localization framework for the Endurance mission. Future works include comparing the state estimation performance when using two satellites for localization and investigating the scenario where the Endurance rover is moving during the measurement window.

ACKNOWLEDGEMENTS

This research is supported by the NSF Graduate Research Fellowship No. DGE-2146755 and the Stanford Knight-Hennessy Scholars graduate fellowship. We would like to acknowledge Keidai Iiyama for the insightful discussions. We would also like to thank the rest of the Stanford Navigation and Autonomous Vehicles Laboratory for their helpful feedback and support.

REFERENCES

Audet, Y., Melman, F. T., Molli, S., Sesta, A., Plumaris, M., Psychas, D., Swinden, R., Girodano, P., and Ventura-Traveset, J. (2024). Positioning of a Lunar Surface Rover on the South Pole Using LCNS and DEMs. *Advances in Space Research*.

Bhamidipati, S., Mina, T., and Gao, G. (2022). A Case Study Analysis for Designing a Lunar Navigation Satellite System with Time-Transfer from Earth-GPS. *Proceedings of the Institute of Navigation ITM conference (ION ITM 2022)*.

Borio, D., Sokolova, N., and Lachapelle, G. (2011). Doppler measurement accuracy in standard and high-sensitivity global navigation satellite system receivers. *IET Radar, Sonar and Navigation*, 5(6):657–665.

Cauligi, A., Swan, R. M., Ono, H., Daftry, S., Elliot, J., Matthies, L., and Atha, D. (2023). ShadowNav: Crater-Based Localization for Nighttime and Permanently Shadowed Region Lunar Navigation. *2023 IEEE Aerospace Conference*.

Cortinovis, M., Mina, T., and Gao, G. (2024). Assessment of Single Satellite-based Lunar Positioning for the NASA Endurance Mission. *2024 IEEE Aerospace Conference*.

Daftry, S., Chen, Z., Cheng, Y., Tepsuporn, S., Khattak, S., and Matthies, L. (2023). LunarNav: Crater-based Localization for Long-range Autonomous Lunar Rover Navigation. *2023 IEEE Aerospace Conference*.

Delépaut, A., Giordano, P., Ventura-Traveset, J., Blonski, D., Schönfeldt, M., Schoonejans, P., Aziz, S., and Walker, R. (2020). Use of GNSS for lunar missions and plans for lunar in-orbit development. *Advances in Space Research*, 66(12):2739–2756.

Folta, D., Bosanac, N., Elliott, I., Mann, L., Mesarch, R., and Rosales, J. (2022). Astrodynamics Convention and Modeling Reference for Lunar, Cislunar, and Libration Point Orbits. (NASA/TP-20220014814). *NASA, Technical Publication*.

Iiyama, K., Bhamidipati, S., and Gao, G. (2023). Terrestrial GPS Time-Differenced Carrier-Phase Positioning of Lunar Surface Users. *2023 IEEE Aerospace Conference*.

Jun, W. W., Cheung, K.-M., and Lightsey, E. G. (2023). Improved Surface Positioning with Measurement Differences in Joint Doppler and Ranging. *2023 IEEE Aerospace Conference*.

Kaplan, E. D. and Hegarty, C. (2017). *Understanding GPS/GNSS: Principles and Applications*. Artech House.

Keane, J. T., Tikoo, S. M., and Elliot, J. (2022). Endurance: Lunar South Pole-Aitken Basin Traverse and Sample Return Rover. *NASA Jet Propulsion Laboratory, Technical Report*.

Kershner, R. B. and Newton, R. R. (1962). The Transit System. *The Journal of Navigation*, 15(2):129–144.

Krawinkel, T. and Schön, S. (2016). Benefits of receiver clock modeling in code-based GNSS navigation. *GPS Solutions*, 20:687–701.

Melman, F. T., Zoccarato, P., Orgel, C., Swinden, R., Giordano, P., and Ventura-Traveset, J. (2022). LCNS Positioning of a Lunar Surface Rover Using a DEM-Based Altitude Constraint. *Remote Sensing*, 14(16):3942.

Misra, P. and Enge, P. (2012). *Global Positioning System: Signals, Measurements & Performance*. Ganga-Jamuna Press.

Nardin, A., Minetto, A., Guzzi, S., Dovis, F., Konitzer, L., and Parker, J. J. K. (2023). Snapshot Tracking of GNSS Signals in Space: A Case Study at Lunar Distances. *Proceedings of the 36th International Technical Meeting of the Satellite Division of The Institute of Navigation (ION GNSS+ 2023)*, pages 3267–3281.

NASA (2022). Lunar communications relay and navigation systems (LCRNS). *Preliminary Lunar Relay Services Requirements Document (SRD)*.

NASA (2022). NASA's Lunar Exploration Program Overview. *NASA, Technical Report*.

O'Dea, A., Kinman, P., Pham, T. T., and Chang, C. (2019). Doppler tracking. *Deep Space Network, DSN No. 810-005, 202, Rev. C*.

Psiaki, M. L. (2021). Navigation using carrier Doppler shift from a LEO constellation: TRANSIT on steroids. *NAVIGATION: Journal of the Institute of Navigation*, 68(3):621–641.

Schmittberger, B. L. and Scherer, D. R. (2020). A Review of Contemporary Atomic Frequency Standards. *arXiv preprint arXiv:2004.09987*.

SSTL (2022). Lunar Pathfinder: Data relay satellite in orbit around the Moon. *SSTL, Service Guide (V4)*.